Cell

Retinal Input Instructs Alignment of Visual Topographic Maps

Jason W. Triplett,[1] Melinda T. Owens,[2] Jena Yamada,[1] Greg Lemke,[3] Jianhua Cang,[4] Michael P. Stryker,[2] and David A. Feldheim[1,*]

[1]Department of Molecular, Cell, and Developmental Biology, University of California, Santa Cruz, Santa Cruz, CA 95064, USA
[2]W.M. Keck Foundation Center for Integrative Neuroscience, Department of Physiology, University of California, San Francisco, San Francisco, CA 94143, USA
[3]Molecular Neurobiology Laboratory, The Salk Institute for Biological Studies, La Jolla, CA 92037, USA
[4]Department of Neurobiology and Physiology, Northwestern University, Evanston, IL 60208, USA
*Correspondence: feldheim@biology.ucsc.edu
DOI 10.1016/j.cell.2009.08.028

SUMMARY

Sensory information is represented in the brain in the form of topographic maps, in which neighboring neurons respond to adjacent external stimuli. In the visual system, the superior colliculus receives topographic projections from the retina and primary visual cortex (V1) that are aligned. Alignment may be achieved through the use of a gradient of shared axon guidance molecules, or through a retinal-matching mechanism in which axons that monitor identical regions of visual space align. To distinguish between these possibilities, we take advantage of genetically engineered mice that we show have a duplicated functional retinocollicular map but only a single map in V1. Anatomical tracing revealed that the corticocollicular projection bifurcates to align with the duplicated retinocollicular map in a manner dependent on the normal pattern of spontaneous activity during development. These data suggest a general model in which convergent maps use coincident activity patterns to achieve alignment.

INTRODUCTION

The ability to analyze multiple attributes of the external environment allows for a robust comprehension of the outside world, but the means by which attributes from distinct sources are bound together in the brain presents a significant challenge for neuroscience (Mesulam, 1998; Treisman, 1996). Vision provides information about the size, shape, color, and motion of perceived objects, and each of these qualities may be processed in separate areas prior to integration (Felleman and Van Essen, 1991; Wolfe and Cave, 1999). Neuronal connections responsible for processing visual information are often organized as orderly topographic maps, in which neighbor-neighbor relationships are maintained between brain areas (Chklovskii and Koulakov, 2004; Luo and Flanagan, 2007). Over the past decade, a great deal of work has elucidated many of the molecular and activity-dependent mechanisms responsible for the development of topographic maps (Huberman et al., 2008a). However, little is known about how topographic maps from different brain regions are merged in associative areas.

The mouse superior colliculus (SC) is an integrative midbrain center that controls reflexive head and eye movements. The SC is organized into several layers, each of which has distinct sources of innervation and afferent targets (May, 2005). Retinal ganglion cells (RGCs) project to the dorsal-most layer of the SC, the upper stratum griseum superficiale (SGS), and are organized topographically, such that the nasal-temporal (N-T) axis of the retina projects to the anterior-posterior (A-P) axis of the SC and the dorsal-ventral (D-V) axis of the retina projects along the medial-lateral (M-L) axis of the SC. The SC also receives visual input from the primary visual cortex (V1). V1 axons terminate in a deeper layer of the SGS (lower SGS) and are organized such that they are in register with the retinocollicular map (Dräger and Hubel, 1976). This corticocollicular projection provides a link between the two major streams of visual processing, the retinocollicular pathway, used for some reflexive visual behaviors, and the retino-geniculo-cortical pathway involved in conscious vision.

Two distinct models can explain how the retinocollicular and corticocollicular maps become aligned in the SC (Figure 1). A gradient-matching model postulates that gradients of molecules expressed by both V1 and RGC axons match graded labels expressed in the SC to specify each map (Figure 1A). In this case, corticocollicular mapping is independent of retinocollicular mapping, but because both projections use information provided by the same target molecules, they become aligned. Consistent with this model, there are complementary gradients of expression of EphAs and ephrin-As along the axes corresponding to the azimuth representation: the N-T axis of the retina, the M-L axis of V1, and the A-P axis of the SC. These countergradients direct topographic mapping, such that areas of high EphA expression project to areas with low ephrin-A expression, and areas of high ephrin-A expression project to areas of low EphA expression (Cang et al., 2005a; Feldheim et al., 1998; Frisén et al., 1998; Luo and Flanagan, 2007; Rashid et al., 2005; and Figure 1A). Therefore, temporal RGCs and lateral V1 projection neurons would project to the same A-P location in the SC because they express similar amounts of EphA receptors.

A retinal-matching model for map alignment proposes that Hebbian-type mechanisms (Hebb, 1949) or direct axon-axon

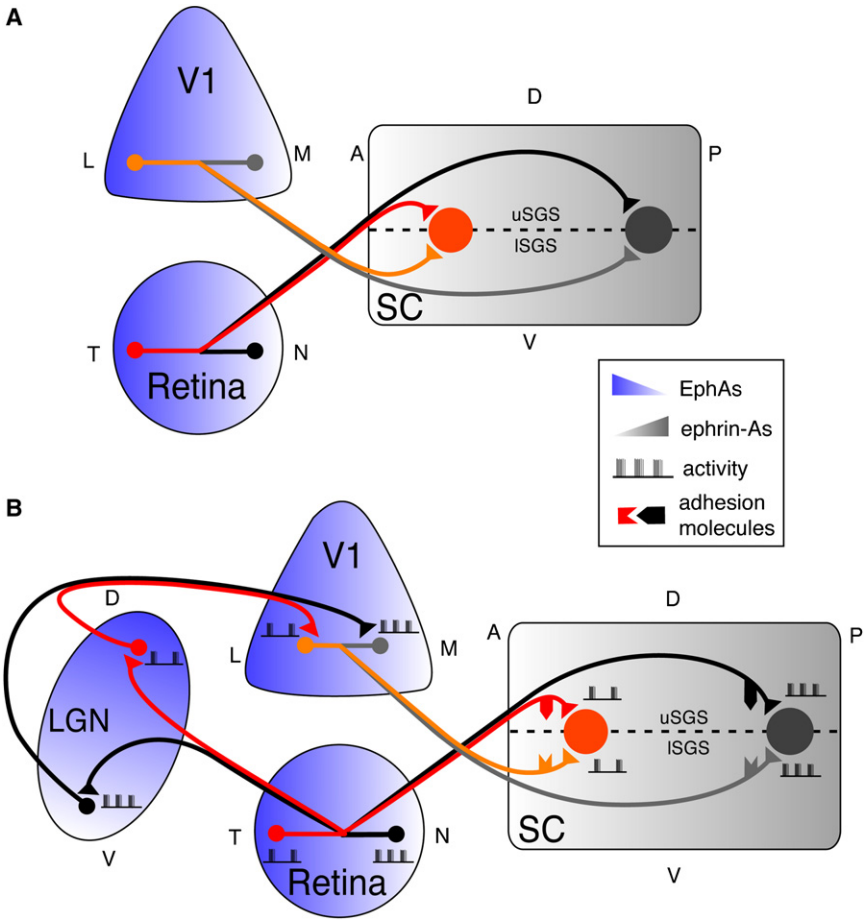

Figure 1. Models of Visual Map Alignment in the Superior Colliculus of the Wild-Type Mouse

(A) Gradient-matching model. Graded expression of EphA receptors (blue) in both the retina and primary visual cortex (V1) are used to guide topographic mapping in the superior colliculus (SC), which expresses repulsive ephrin-A ligands (gray) in a gradient in both recipient layers. N, nasal; T, temporal; A, anterior; P, posterior; D, dorsal; V, ventral; L, lateral; M, medial; uSGS, upper stratum griseum superficiale; lSGS, lower stratum griseum superficiale.

(B) Retinal-matching model. Retinocollicular mapping is established first through the use of graded EphAs and ephrin-As. Then, V1 projection neurons terminate in areas with similar activity patterns or with RGCs expressing complementary cell surface molecules.

interactions are used to direct V1 and RGC axons that monitor the same point in space to terminate in the same region of the SC (Figure 1B). In this model, the retinocollicular map is first established by a gradient-matching mechanism. V1 axons would then form synapses with SC neurons onto which RGCs that share common activity patterns or cell surface molecules synapse. In support of this model, it has been shown that retinal input can be instructive for the alignment of auditory and visual maps in the owl tectum and ferret SC (King et al., 1988; Knudsen and Brainard, 1991). Additionally, in the peripheral nervous system, axon-axon signaling is used to direct the convergent innervation of motor and sensory neuron axons onto a common muscle target (Gallarda et al., 2008).

Here, we show that *Islet2-EphA3* knockin (EphA3$^{ki/ki}$) mice (Brown et al., 2000), have two functional maps in the SC, but a single functional map in V1, providing a tool to distinguish between these models. We find that corticocollicular projections align with both of the duplicated retinocollicular maps in EphA3$^{ki/ki}$ mice, suggesting that retinal input is instructive for corticocollicular topography and map alignment. In support of this, we find that alignment occurs after the retinal map is established but before eye opening, and that reduction or removal of retinal input alters corticocollicular mapping. Furthermore, we show that disruption of spontaneous cholinergic retinal waves in EphA3$^{ki/ki}$ mice prevents map alignment. Taken together, these data suggest that the V1 projection aligns with a pre-existing retinocollicular map by matching activity patterns.

RESULTS

Islet2-EphA3 Knockin Mice Have a Duplicated Azimuth Map in the SC, but Not V1

One of the most striking experiments that demonstrated the importance of EphA receptors in topographic mapping of the retinocollicular projection comes from Brown and colleagues, who showed that EphA3$^{ki/ki}$ mice have duplicated anatomical maps in the SC (Brown et al., 2000). EphA3$^{ki/ki}$ mice ectopically express EphA3 from an internal-ribosome-entry-site cDNA expression cassette placed in the 3′ untranslated region of the *Islet2* gene. This drives expression of EphA3 in about 40% of RGCs scattered in a salt-and-pepper fashion across the retina (Brown et al., 2000), and results in the retina having two populations of RGCs: (1) an Islet2^{-} population that expresses endogenous EphA levels, and (2) an Islet2^{+} population that has EphA3 expression superimposed on top of the endogenous EphA levels. Because RGCs sort topographically along the A-P axis of the SC based on relative EphA levels, these mice have duplicated azimuth maps in the SC, as assessed by anatomical tracing (Brown et al., 2000; Reber et al., 2004).

We asked if the duplicated anatomical maps in these mice were functional, or if instead one of the maps became silenced. To distinguish between these possibilities we used a Fourier method for imaging of intrinsic optical signals of neural activity to visualize the functional maps in the mouse SC (Cang et al., 2008b; Kalatsky and Stryker, 2003). In this method, drifting thin bars are presented on a video monitor placed 25 cm away from an anesthetized mouse, contralateral to the SC being imaged. The bars were swept along the D-V or N-T axes to stimulate constant lines of elevation or azimuth, respectively. By extracting the optical signal at the stimulus frequency, we

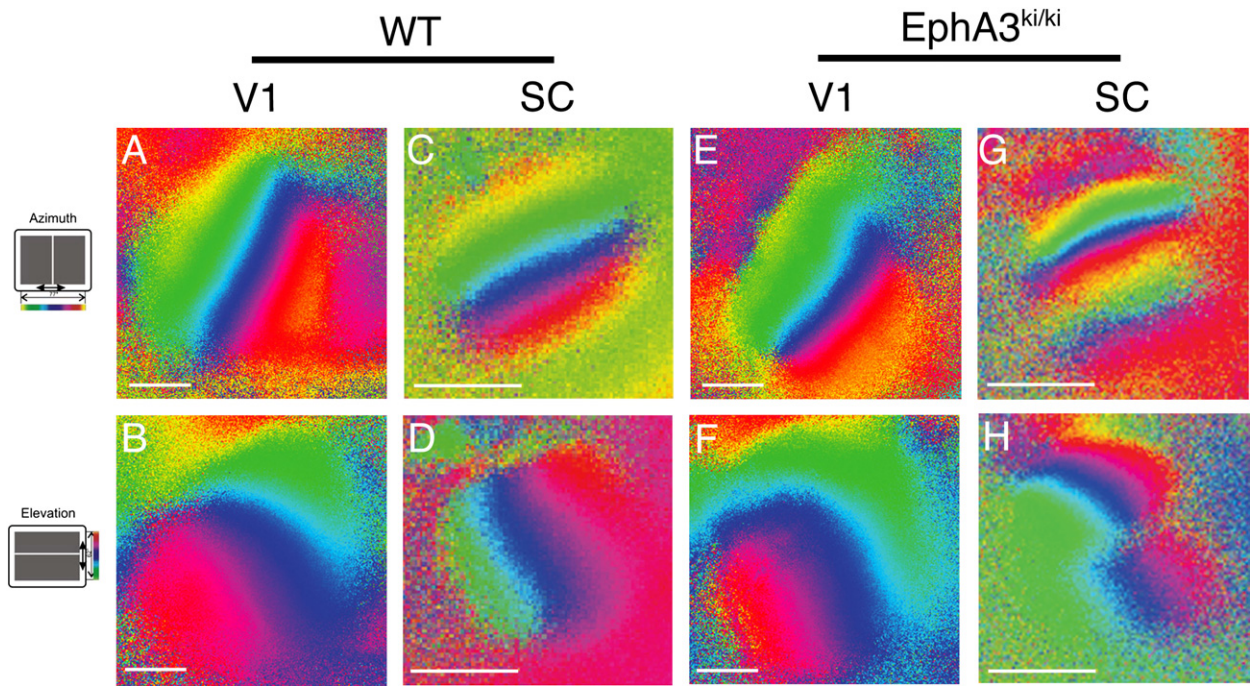

Figure 2. EphA3$^{ki/ki}$ Mice Have Duplicated Functional Maps in the SC and a Single Functional Map in V1

(A–D) Intrinsic optical imaging signal obtained from V1 (A and B) and SC (C and D) of WT adult mice presented a drifting bar stimulus along the azimuth (A and C) or elevation (B and D) axis. Scale bar represents 500 μm.

(E–H) Intrinsic optical imaging signal obtained from V1 (E and F) and SC (G and H) of EphA3$^{ki/ki}$ animals presented a drifting bar stimulus along the azimuth (E and G) or elevation (F and H) axis. Scale bar represents 500 μm.

computed the response magnitude and timing in relation to the stimulus cycle, which can then be converted to the location in visual field. Using this method, we found that wild-type (WT) mice have functional topography along both the azimuth and elevation axes to form single, continuous maps in both the SC and V1 (Figures 2A–2D). By contrast, in EphA3$^{ki/ki}$ mice there were two complete and continuous maps of azimuth (along the A-P axis of the SC) (Figure 2G), which are generally consistent with the anatomical maps of Brown et al. (2000). Each of the maps occupied about half of the SC; however, we detected a stronger signal from the anterior compared to the posterior map (see Figure S1 available online). Imaging of the elevation axis (along the M-L axis of the SC) showed that its map did not duplicate, but a discontinuity in the representation of elevation was observed at the border between the two azimuthal maps (Figure 2H). As a result, the SCs of EphA3$^{ki/ki}$ mice contain two complete maps of the visual field, each with a full representation of azimuth and elevation.

We next asked if the functional V1 map is duplicated in EphA3$^{ki/ki}$ mice. To determine this, we used the same imaging procedure and found that there was always a single topographic map in V1 of EphA3$^{ki/ki}$ mice, similar to those observed in WT animals (Figure 2A, 2B, 2E, and 2F). Therefore, while EphA3$^{ki/ki}$ mice have a duplicated functional map along the N-T mapping axis of the visual field in the SC, they have a single functional map in V1.

In theory, a single functional map in V1 could arise if an early anatomically duplicated map were somehow repaired by the intrinsic connections in the cortex or if one map were silenced, resulting in a single functional map when one measures the responses of cortical cells. To test this possibility, we performed anatomical tracing experiments to determine whether the retinogeniculate and geniculo-cortical projections were duplicated anatomically. We anterogradely labeled subsets of RGCs projecting to the lateral geniculate nucleus (LGN) of the thalamus, and retrogradely labeled LGN cells by injection of tracer in their terminal arbors in V1. In neither case did we find a duplication of the maps (Figure S2). These anatomical findings are consistent with the functional data, showing that RGC axons in EphA3$^{ki/ki}$ mice do not form a duplicated map in the retino-geniculo-cortical pathway.

V1 Projections Split to Align with a Duplicated SC Map in EphA3$^{ki/ki}$ Mice

The fact that EphA3$^{ki/ki}$ mice have a single map in V1 but a duplicated map in the SC allowed us to test models of map alignment in the SC. Because there is ectopic EphA3 expression in RGCs, but not in either V1 or the SC, a gradient-matching model predicts that a single injection of DiI into V1 would trace axons that terminate in the topographically appropriate position of the SC, which would result in a misalignment of the V1 and SC maps. However, a retinal-matching model for alignment predicts that V1 terminations in the SC will align with those of RGC terminations that monitor the identical region of visual space. In this model, a single injection of DiI into V1 of EphA3$^{ki/ki}$ mice would result in two termination zones (TZs) in the SC, with neither TZ

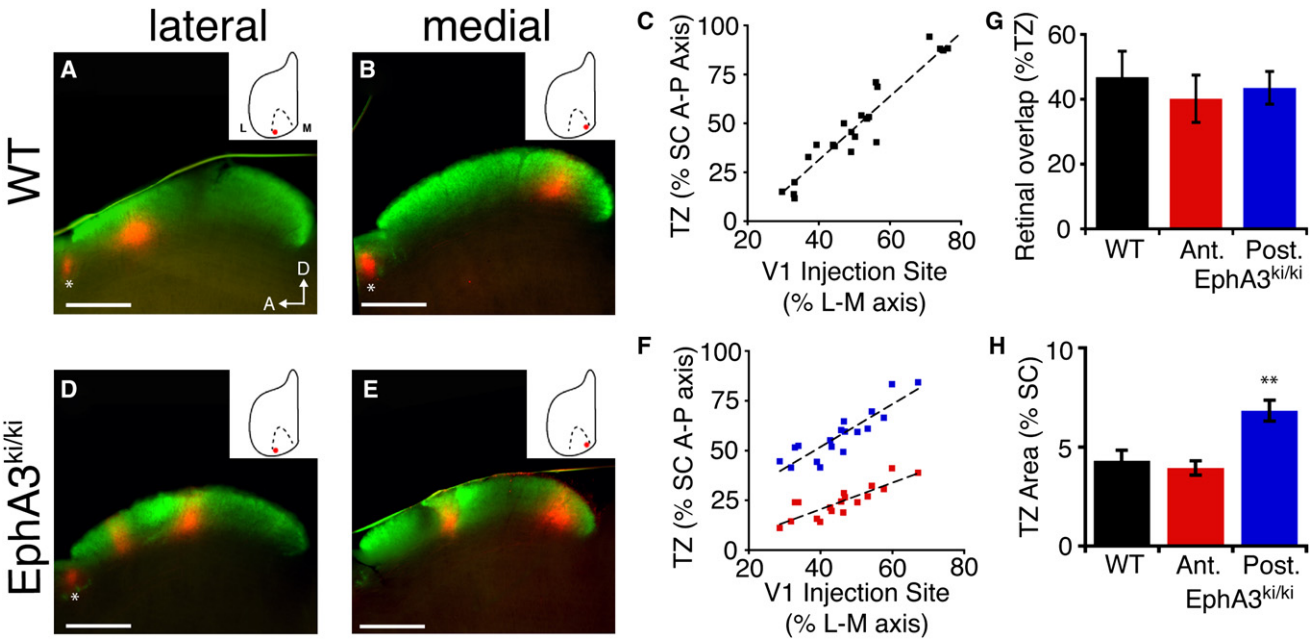

Figure 3. V1-SC Projections Form Two Termination Zones in EphA3$^{ki/ki}$ Mice

(A and B) Parasagittal sections of the SC after focal injection of DiI (red) in V1 and whole eye fill with CTB-488 (green) in the contralateral eye, which labels all RGCs. In WT mice lateral V1 injections result in TZs in the anterior SC, while medial V1 injections give rise to TZs in the posterior SC. *Inserts*: Schematic of V1 injection site; scale bar represents 500 μm; L, lateral; M, medial; A, anterior; D, dorsal; *, pretectal nucleus.

(C) Corticocollicular TZ location expressed as a percent of SC anterior-posterior axis plotted against the V1 injection site, expressed as percent of the lateral-medial axis of the cortical hemisphere. Line represents best-fit regression, $R^2 = 0.9135$, n = 23.

(D and E) Parasagittal SC sections after focal injection of DiI (red) in V1 and whole eye fill with CTB-488 (green) in the contralateral eye, which labels all RGCs. In EphA3$^{ki/ki}$ mice lateral V1 injections result in two termination zones in the anterior and central SC, whereas medial injections result in two termination zones in the central and posterior SC. *Inserts*: Schematic of V1 injection site; scale bar represents 500 μm; *, pretectal nucleus.

(F) Corticocollicular TZ location expressed as a percent of SC anterior-posterior (A-P) axis plotted against the V1 injection site expressed as percent of the lateral-medial (L-M) axis of the cortical hemisphere. Line represents best-fit regression, $R^2 = 0.7828$ and 0.7131 for posterior (blue) and anterior (red) TZs, respectively; n = 18.

(G) Quantification of corticocollicular TZ overlap with the retinal recipient layer in WT and EphA3$^{ki/ki}$ mice. Data are represented as mean and standard error of the mean (SEM), n > 10.

(H) Quantification of corticocollicular TZ area expressed as a percent of SC area in WT and EphA3$^{ki/ki}$ mice. Data are represented as mean ± SEM, n = 18. **p < 0.01 by ANOVA and Tukey's HSD post-hoc analysis.

in the position that would normally be topographically appropriate. To distinguish between these possibilities, we injected DiI focally into V1 of adult (>postnatal day 40 or P40) mice and visualized the V1 terminations in parasagittal SC sections that reveal the N-T mapping axis. In some mice we also labeled all of the contralateral RGC inputs into the SC by injecting fluorescein-conjugated cholera toxin B (CTB-488) into the eye. Corticocollicular TZs were observed in the lower SGS, but we found they overlapped significantly with projections from the retina, because nearly half (46.8% ± 8.0%) of corticocollicular TZ area fell within the region of retinal input (Figure 3G). In adult WT mice, we found that V1 projection neurons map topographically within the SC such that neurons in medial, central, and lateral V1 project to the posterior, central, and anterior SC, respectively, with a linear relationship between V1 injection site and SC TZ location ($R^2 = 0.9135$, N = 23) (Figures 3A–3C).

In contrast to the findings in WT mice, a single injection into V1 of EphA3$^{ki/ki}$ mice always resulted in two TZs in the SC rather than one (18/18 mice) (Figures 3D–3F). Quantification of injection site and TZ locations revealed that V1 axons split into two topographic maps ($R^2_{ant} = 0.7131$, $R^2_{post} = 0.7828$) (Figure 3F). Interestingly, the posterior TZs were approximately twice the area (1.89 ± 0.21-fold) of the anterior TZs, which were similar in size to WT TZs (Figure 3H), suggesting that refinement of the posterior map was incomplete. This difference was consistent with the weaker signal from the posterior map as compared with the anterior map observed during our functional imaging experiments (Figure S1), suggesting there might also be a correlation between retinal input strength and corticocollicular refinement. However, posterior-projecting V1 neurons did not make errors in laminar localization, because overlap with the retinal input layer was similar to that seen in anterior TZs and WT TZs (Figure 3G).

Retinal Input Is Required for Precise Topographic Mapping and Refinement of Corticocollicular Projections

Our functional imaging and anatomical tracing studies in EphA3$^{ki/ki}$ mice suggest an instructive role for RGC input in the alignment of retinocollicular and corticocollicular maps. Previous

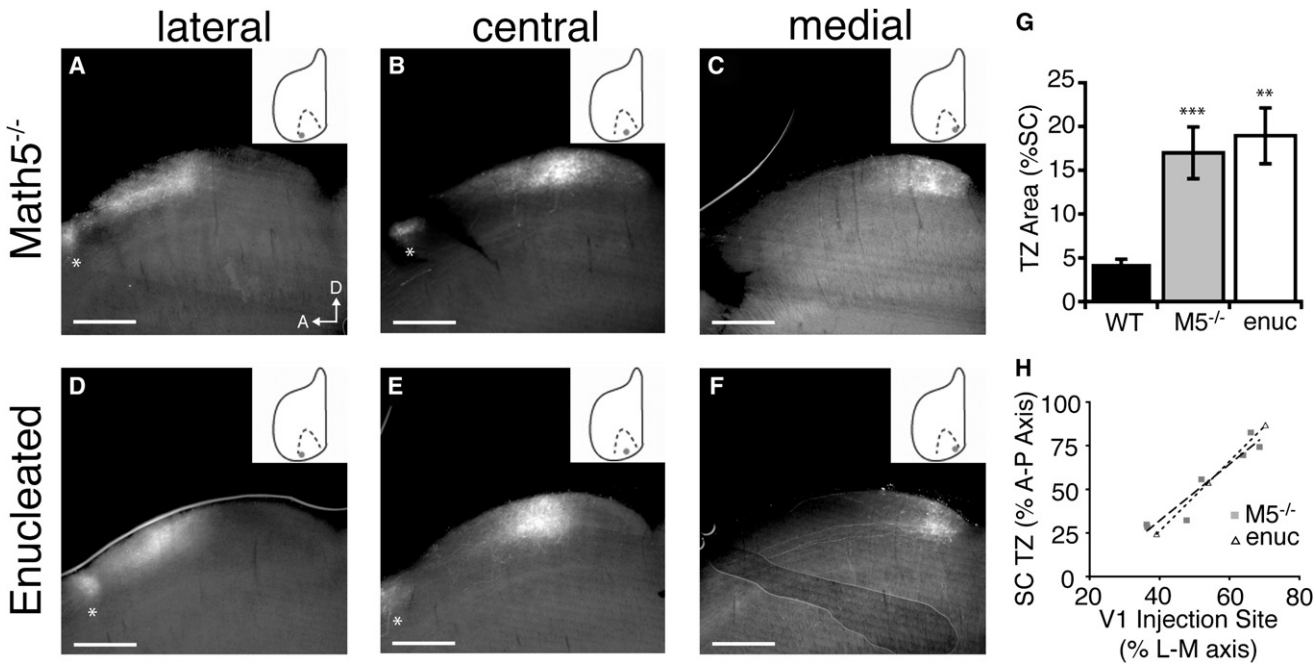

Figure 4. Retinal Input Is Required for Precise Topography of the Corticocollicular Projection

(A–C) Parasagittal SC sections after focal injection of DiI (white) in V1. In Math5$^{-/-}$ mice, injections in lateral, central, and medial V1 result in broad TZs in anterior, central, and posterior SC, respectively. *Inserts*: Schematic of V1 injection site; scale bar represents 500 μm; *, pretectal nucleus; A, anterior; D, dorsal.

(D–F) Parasagittal SC sections after focal injection of DiI (white) in V1. In adult WT mice that were enucleated at P6, injections in lateral, central and medial V1 result in broad TZs in anterior, central, and posterior SC, respectively. *Inserts*: Schematic of V1 injection site; scale bar represents 500 μm; *, pretectal nucleus; A, anterior; D, dorsal.

(G) Quantification of TZ size as a percent of the SC in WT, Math5$^{-/-}$, and enucleated mice. Data are represented as mean ± SEM, n > 3 for each group; because data from anterior and posterior TZs were not significantly different (p = 0.4, n > 3), these data were pooled. ***p < 0.001 versus WT; **p < 0.01 versus WT, Kolmogorov-Smirnov test.

(H) Corticocollicular TZ location expressed as a percent of SC anterior-posterior (A-P) axis was plotted against the V1 injection site expressed as percent of the lateral-medial (L-M) axis of the cortical hemisphere for Math5$^{-/-}$ (gray squares) and enucleated mice (open triangles). Line represents best-fit regression, R^2 = 0.9139 for Math5$^{-/-}$ and R^2 = 1 for enucleated.

studies have shown that removal of retinal input during development or adulthood results in increased corticocollicular plasticity (García del Caño et al., 2002), and that anophthalmic mice have broader corticocollicular TZs compared with WT controls (Khachab and Bruce, 1999). However, neither of these studies performed a detailed analysis of the topographic organization of V1 projections.

To determine whether retinal input was required for V1 projection topography, we assessed corticocollicular maps in two kinds of mice in which the retinal input to the SC is reduced: (1) mice lacking Math5, a basic-helix-loop-helix transcription factor essential for RGC differentiation (Brown et al., 2001), and (2) monocularly enucleated WT mice. Math5 mutant mice have approximately 5%–10% of wild-type levels of RGCs (Lin et al., 2004). These remaining RGCs project to the anterior medial SC and only fill approximately 35% of the SC (C. Pfeiffenberger, J.W.T., and D.A.F., unpublished data). Corticocollicular TZs were approximately four times as large in Math5$^{-/-}$ and enucleated mice compared with WT controls (17.0% ± 3.0% and 18.9% ± 3.2% versus 4.3% ± 0.5%) (Figures 4A–4G). However, rough topography remained intact in both of these mice, with a linear relationship between V1 injection site and the center of the TZ location in the SC (R^2 = 0.9139, N = 7, Math5$^{-/-}$; R^2 = 1, n = 3, enucleated) (Figure 4H). Taken together, these data suggest that when retinal input is reduced or absent, rough corticocollicular topography remains; however, TZ refinement and precise localization are impaired.

Corticocollicular Mapping Occurs after Retinocollicular Mapping and before Eye Opening

For a retinal-matching mechanism to be used, it is advantageous for the retinocollicular neurons to complete map formation prior to the time when V1 axons refine. Previous studies have shown that many RGC axons initially overshoot their eventual collicular TZ before a process of local branching and pruning refines the axons to their final TZ, which finishes by P8 in the mouse (Hindges et al., 2002; McLaughlin et al., 2003; Figures 5E and 5F). We examined the time course of corticocollicular projection mapping by anatomical tracing. We first observed V1 axons in the SC at P6, where they streamed in without a defined TZ (Figure 5A). Over the next week, V1 axons refine to a final TZ by P12 (Figures 5B–5D and 5G). These data indicate that corticocollicular mapping occurs after the retinocollicular map has formed and before eye opening, which occurs at P14–15. Also, they are

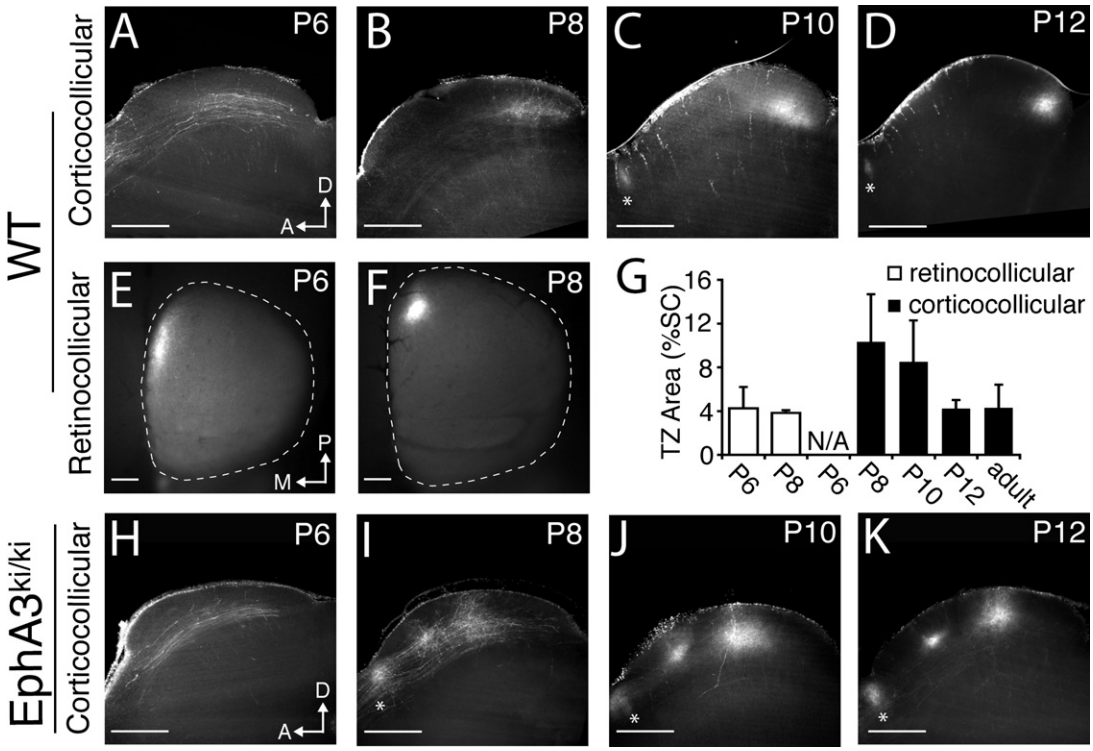

Figure 5. Time Course of Corticocollicular Mapping in WT and EphA3$^{ki/ki}$ Mice

(A–D) Parasagittal SC sections after focal injection of DiI (white) in V1. In WT pups corticocollicular axons were observed as early as postnatal day 6 (P6), and a broad TZ was apparent by P8, which refined further at P10 and completed by P12. Scale bar represents 500 μm; *, pretectal nucleus; A, anterior; D, dorsal.

(E and F) Whole-mount SC images after focal injection of DiI (white) in nasal retina. In WT mice, a broad retinocollicular TZ was apparent at P6 (E), which was fully refined by P8 (F). Scale bar represents 500 μm; M, medial; P, posterior.

(G) Quantification of TZ size as a percent of the SC. Data are represented as mean and standard deviation, n > 3 for each group.

(H–K) Parasagittal SC sections after focal injection of DiI (white) in V1. In EphA3$^{ki/ki}$ pups, corticocollicular axons were observed at P6, and broad TZs were apparent by P8, which refined further at P10 and were complete by P12. Scale bar represents 500 μm; *, pretectal nucleus; A, anterior; D, dorsal.

consistent with the idea that V1 axons sort topographically by matching with a retinocollicular map that is already present.

Cholinergic Activity Is Required for Visual Map Alignment in EphA3$^{ki/ki}$ Mice

Before eye opening, spontaneous activity in the form of correlated bursts of action potentials propagates across the retina in a wave-like manner. Retinal waves progress through three distinct developmental stages that differ in their means of propagation. In mice, the earliest waves begin around embryonic day 16 (E16), propagate quickly, occur with high frequency, and are mediated by gap junctions (Firth et al., 2005; Singer et al., 2001; Syed et al., 2004). Between birth and P10 the middle-stage waves rely primarily upon cholinergic neurotransmission between starburst amacrine cells and RGCs. During this time both wave speed and wave frequency are lower compared with embryonic waves (Bansal et al., 2000; Feller et al., 1996; Syed et al., 2004). Late-stage waves (P10–P15+) depend increasingly on glutamatergic neurotransmission between bipolar cells and RGCs, and coincide with increases in wave speed and frequency (Demas et al., 2006; Wong, 1999). To determine which of these types of activity might be important for map alignment, we examined the time course of corticocollicular projection bifurcation in EphA3$^{ki/ki}$ mice. We found that V1 axons reach the SC by P6 and slowly refine to two termination zones by P12 (Figures 5H–5K), similar to the time course seen in WT mice (Figures 5A–5D). This refinement occurs during the end of the cholinergic middle-stage waves and overlaps the period of the glutamatergic late-stage waves, suggesting that one or both of these types of spontaneous activity patterns could be used for map alignment.

To test the requirement for locally correlated neural activity produced by middle-stage waves in corticocollicular map refinement, we examined whether precise alignment of retinocollicular and corticocollicular maps still occurred in β2 nicotinic acetylcholine receptor subunit knockout (β2$^{-/-}$) mice, in which the pattern of spontaneous retinal activity is dramatically altered (Bansal et al., 2000; McLaughlin et al., 2003; Sun et al., 2008; Xu et al., 1999). We find that the corticocollicular topography is disrupted in these mice almost as much as in Math5$^{-/-}$ and enucleated mice. Single injections of DiI into V1 resulted in diffuse TZs, occupying greater than three times the A-P collicular territory as in WT animals (15.5% ± 1.6% versus 4.3% ± 0.5%) (Figures S3A, S3B, and S3D). Interestingly, we observed that the layer specificity of corticocollicular projections was also disrupted in β2$^{-/-}$ mice, since TZs showed less overlap with

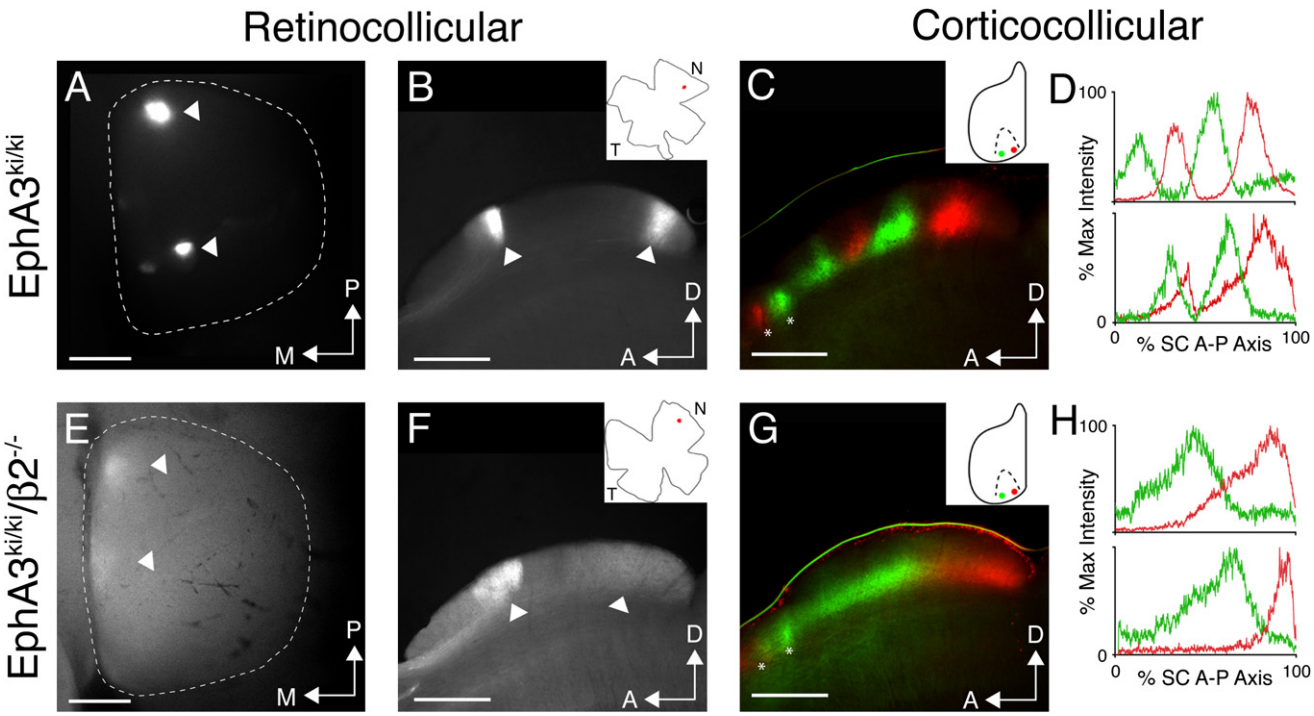

Figure 6. Spontaneous Cholinergic Waves Are Required for Map Alignment in EphA3$^{ki/ki}$ Mice

(A) Whole-mount SC after focal injection of DiI (white) in nasal retina. In EphA3$^{ki/ki}$ mice, two distinct retinocollicular TZs were observed (arrowheads) in the appropriate topographic positions. Scale bar represents 500 μm; M, medial; P, posterior.

(B) Parasagittal section of the SC in (A) revealing two distinct retinocollicular TZs (arrowheads). *Insert*: Schematic of retinal injection site; scale bar represents 500 μm; A, anterior, D, dorsal. Images in (A) and (B) are from the same SC.

(C) Parasagittal SC section after focal injection of DiI (red) and DiA (green) in V1. In EphA3$^{ki/ki}$ mice, each single injection results in two corticocollicular TZs, which are interdigitated. *Insert*: Schematic of V1 injection sites; scale bar represents 500 μm; *, pretectal nucleus; A, anterior; D, dorsal.

(D) Representative intensity profile plots from two EphA3$^{ki/ki}$ mice after focal injection of DiI (red) and DiA (green) in V1.

(E) Whole-mount SC after focal injection of DiI (white) in nasal retina. In EphA3$^{ki/ki}$/β2$^{-/-}$ mice, showing two broad TZs (arrowheads). Scale bar represents 500 μm; M, medial; P, posterior.

(F) Parasagittal section of the SC in (D) showing two broad TZs (arrowheads). *Insert*: Schematic of retinal injection site; scale bar represents 500 μm; A, anterior; D, dorsal. Images in (D) and (E) are from the same SC.

(G) Parasagittal SC section after focal injection of DiI (red) and DiA (green) in V1. In EphA3$^{ki/ki}$/β2$^{-/-}$ mice, each single injection results in a single, broad TZ, which are not interdigitated. *Insert*: Schematic of V1 injection sites; scale bar represents 500 μm; *, pretectal nucleus; A, anterior; D, dorsal.

(H) Representative intensity profile plots from two EphA3$^{ki/ki}$/β2$^{-/-}$ mice after focal injection of DiI (red) and DiA (green) in V1.

retinocollicular projections compared to WT (24.9% ± 6.3% versus 46.8% ± 8.0%) (Figure S3E). However, rough topography was maintained in β2$^{-/-}$ mice (R^2 = 0.9118, n = 10) (Figure S3D), similar to the retinocollicular phenotype observed in these mice (Chandrasekaran et al., 2005).

To determine the precise role of cholinergic spontaneous activity in the alignment of V1 and retinal projections, we crossed the β2$^{-/-}$ mice with EphA3$^{ki/ki}$ mice to create combination mutants (EphA3$^{ki/ki}$/β2$^{-/-}$). Analysis of retinocollicular mapping in these mice revealed that they retained a duplicated map, although each TZ was somewhat broader (Figures 6E and 6F). If map alignment did not depend on the locally correlated activity produced by cholinergic waves and was instead driven by other mechanisms, two broader TZs would be expected from a single V1 labeling. Alternatively, if β2-dependent waves were required for map alignment, we would expect a single rather than a duplicated corticocollicular map, such that labeling of V1 neurons would result in a single, broad TZ in the SC. In every case, we detected only a single, broad TZ for each V1 injection in EphA3$^{ki/ki}$/β2$^{-/-}$ mice (Figures 6G and 6H). Use of two colors to label the origin of two different V1 projection populations revealed that the map was indeed singular, because there was no interdigitation of TZs, as was always observed in EphA3$^{ki/ki}$ mice in which cholinergic activity was not altered (Figures 6C and 6D). These data are consistent with a role for cholinergic middle-stage waves in the retinal instruction of corticocollicular map alignment.

DISCUSSION

In these experiments we have used the projection from V1 to the SC as a model to investigate the mechanisms by which sensory maps become aligned during development. Using a combination of anatomical tracing and functional imaging techniques, we found that the EphA3$^{ki/ki}$ mouse has a duplicated functional map along the azimuth axis in the SC but has only a single

map in V1. Remarkably, the corticocollicular projections in this mouse compensate perfectly for this discrepancy and project to both SC maps to maintain alignment. Both the refinement of the corticocollicular map and its splitting in animals with a duplicated retinocollicular map take place after retinocollicular map refinement and before eye opening. Alignment is blocked in mice that lack the normal pattern of spontaneous retinal activity. Taken together, these results demonstrate that that the visual maps in the cortex and SC are aligned in a multistep process. First, the primary visual connections to the SC and LGN and from the LGN to V1 form topographic maps using a combination of mapping labels, patterned retinal activity, and axon competition, and are well refined by P8 (Cang et al., 2008b; Hindges et al., 2002; McLaughlin et al., 2003; Pfeiffenberger et al., 2006). Following this, V1 neurons project to the SC and are oriented and guided to their normal area of the SC using molecular cues, such as Ephs and ephrins. These axons finally refine to areas of the SC that share similar activity patterns generated by retinal waves.

Functional Duplication of the Azimuth Representation in the SC but Not V1 of EphA3$^{ki/ki}$ Mice

The generation of EphA3$^{ki/ki}$ mice allowed for a detailed understanding of the role of graded labels in the development of the retinocollicular map (Brown et al., 2000; Reber et al., 2004). In these mice, EphA3 is expressed in RGCs that normally express Islet2, which leads to the ectopic expression of EphA3 in about half of all RGCs. As a result, immediately adjacent RGCs can have drastically different total EphA receptor expression levels. These RGCs now project to different SC locations, resulting in an overall duplication of the retinocollicular map. These results demonstrate that RGCs sort topographically based on their relative EphA expression level on axons (Brown et al., 2000; Lemke and Reber, 2005). Here, we used a method of intrinsic-signal optical imaging to show that this duplicated map is functional, with each map maintaining smooth topography. Although the azimuth map was duplicated, the elevation representation in the SC remained singular in these mice. These data clearly demonstrate that each axis is mapped independently, in a Cartesian manner, as originally posited by Sperry in his chemoaffinity hypothesis (Sperry, 1963).

Importantly for this study, we found that, despite the duplicated collicular azimuth map, EphA3$^{ki/ki}$ mice have single, normal anatomical maps in the retinogeniculate and geniculocortical projections and a normal, single, functional map in V1. Why is there no map duplication in the retino-geniculo-cortical pathway? One possibility is that although both the Islet2^{+} and Islet2^{-} RGCs project to the SC, the LGN receives input solely from one of these populations. In this case, one would expect two maps in the SC but only one in the LGN, because the relative EphA receptor gradient expressed by the RGC population projecting to the LGN would not be changed. It is known that Islet2^{+} neurons in WT mice project to both the SC and LGN (Pak et al., 2004). It is possible that either the Islet2^{-} RGCs do not project to the contralateral LGN or that the ectopic EphA3 expression in Islet2^{+} RGCs alters their normal projection pattern. We did not observe any change in the size of the LGN in EphA3$^{ki/ki}$ mice (data not shown), suggesting the latter possibility is unlikely. Another possibility is that activity-dependent mapping mechanisms could fix the anatomical map in the LGN but not the SC, because of a differential dependence of correlated activity in the development of topography (Pfeiffenberger et al., 2006). Future studies will be directed to distinguish between these possibilities.

Our studies also find that the two functional maps occupy an equal portion of the SC, but that visual responses from the posterior map are weaker than those from the anterior or WT maps. In EphA3$^{ki/ki}$ mice, the Islet2^{+} subset of RGCs that project to the anterior half of the SC may be a separate physiological type than Islet2^{-} RGCs. These different classes of RGCs may have different maximal responses to the moving bar stimulus used for functional mapping, which could account for the differences in response seen in the two maps. We also observed that the size of the posterior corticocollicular TZ in EphA3$^{ki/ki}$ mice is always larger than the anterior TZ. Because the posterior functional map is weaker relative to the anterior map, this may be the result of a homeostatic mechanism that regulates corticocollicular synapse formation in the SC, as has been demonstrated previously for retinocollicular input (Chandrasekaran et al., 2007). Future characterization of the electrophysiological RGC subtypes projecting to each half of the SC in these mice is needed.

The Corticocollicular Projection Aligns with the Retinocollicular Map Using a Retinal-Matching Mechanism

The disparate maps in V1 and the SC in the EphA3$^{ki/ki}$ mice allowed us to distinguish between models of topographic map alignment during development. Gradient-matching models postulate that gradients of molecules expressed by both V1 and RGC axons match with graded labels expressed in the SC to specify each map. In this case we would expect that a focal injection of DiI into V1 would lead to a TZ in the same place as it would in WT mice, which would lead to a misalignment between the V1 and SC maps in EphA3$^{ki/ki}$ mice. Instead we find that a single injection into V1 results in two and only two TZs in the SC. This shows that V1 axons change their termination sites in response to the duplicated retinocollicular map by matching retinal input. Furthermore, in mice with reduced retinal input, either through enucleation or genetic reduction of RGC number in Math5$^{-/-}$ mice, corticocollicular mapping was disrupted. In both of these cases, we observed overall rough topography of corticocollicular TZs, showing that corticocollicular neurons may also use SC-derived cues to form rough topography.

Retinal input could, in theory, be matched by using common activity patterns shared by V1 neurons and RGCs or be matched using cell surface proteins expressed on V1 and RGC axons. There is a precedence for molecular interactions between axons playing an important role in axon guidance (Gallarda et al., 2008; Pittman et al., 2008), and corticocollicular projections are located such that it is possible they may interact with RGC axons. One mechanism could involve EphA/ephrin-A interactions between V1 and RGC axons. Nasal RGCs express high levels of ephrin-A, so the collicular ephrin-A gradient would be altered in EphA3$^{ki/ki}$ mice by central-projecting nasal axons.

However, we do not observe an obvious change in EphA or ephrin-A gradients in these mice, suggesting the contribution of RGC axon-localized ephrin-As is minor compared with the SC-derived expression (Figure S4). It is also possible that other, yet unidentified molecules that could serve this function might be duplicated in the SC of EphA3$^{ki/ki}$ mice.

Spontaneous Activity Patterns Are Used to Align the Corticocollicular Projection

The time-course of the establishment of the corticocollicular projection in WT and EphA3$^{ki/ki}$ mice shows that refinement occurs before the emergence of vision and during a period when RGCs fire bursts of patterned, spontaneous activity, called retinal waves. This timing overlaps with the end of cholinergic waves and the beginning of the glutamatergic wave period (Huberman et al., 2008a). Cholinergic waves are required for topographic mapping in the retinocollicular, retinogeniculate, and geniculocortical projections (Cang et al., 2008a; McLaughlin et al., 2003; Pfeiffenberger et al., 2006), suggesting that these bursts carry topographic information that filter through the visual circuit. To test if cholinergic retinal waves are used by the V1 projection to align with the retinocollicular projection, we labeled the V1 projection in EphA3$^{ki/ki}$/$\beta2^{-/-}$ combination mutants. $\beta2^{-/-}$ mice have severely altered patterns of spontaneous retinal activity during the first postnatal week, resulting in retinocollicular TZs that fail to refine normally (Chandrasekaran et al., 2005; McLaughlin et al., 2003). In EphA3$^{ki/ki}$/$\beta2^{-/-}$ mutants, retinocollicular TZs are broad, but still duplicate along the A-P axis of the SC. Remarkably, we find that corticocollicular projections in EphA3$^{ki/ki}$/$\beta2^{-/-}$ mice do not bifurcate in the SC, indicating they are misaligned with the retinocollicular map and implicating a role for β2-dependent cholinergic activity in map alignment. Because the β2 mutation is a global knockout the exact contributions of retinal and cortical cholinergic activity cannot be distinguished at this time. It is likely that the refinement defects seen in $\beta2^{-/-}$ mice are due to its action in the retina, since intraocular injection of epibatidine results in a similar phenotype (Cang et al., 2005b; Chandrasekaran et al., 2005). Supporting this view is the observation that transgenic expression of the wild-type β2 gene in the retina of $\beta2^{-/-}$ mice rescues the retinotopic refinement defects in the SC and LGN (M.C. Crair, personal communication). More broadly, any perturbation to retinal activity is also likely to affect cortical activity, although the visual cortex does maintain spontaneous activity following enucleation (Chiu and Weliky, 2001).

Interestingly, we also observed that corticocollicular TZs in $\beta2^{-/-}$ mice show significantly less overlap with the retinal recipient layer than do WT TZs. This suggests that corticocollicular lamination is also dependent on cholinergic spontaneous activity. These data are in contrast to recent studies in mammalian and zebrafish models, which found that RGC lamination in the SC/tectum was not changed when activity was altered or blocked (Huberman et al., 2008b; Nevin et al., 2008). Perhaps the shared activity patterns of these axons allow them to overcome barriers of cell adhesion proposed as cues to define lamination profiles in the CNS (Sanes and Yamagata, 1999). A possible consequence of this layering defect could be a reduced ability of retinal and cortical axons to interact in the SC. Thus, we cannot rule out the possibility that our results in EphA3$^{ki/ki}$/$\beta2^{-/-}$ mice may be caused by a disruption of this interaction during development. Future studies will be directed at determining the molecular cues guiding corticocollicular projections to their appropriate layer(s) and the influence of activity on the expression and function of these cues.

Conclusions

These experiments demonstrate an instructive role for RGCs in the mapping and alignment of a second, cortical visual projection to the SC. Our data demonstrate a role for spontaneous activity that occurs prior to eye opening in providing this instructive signal, which is necessary for both alignment of visual maps and proper lamination of corticocollular projections. Considering previous studies in barn owls and ferrets suggesting a similar instructive role for visual input in auditory mapping in the midbrain (King et al., 1988; Knudsen and Brainard, 1991), it may be a general rule that convergent inputs to a central structure use concomitant activity to align with the primary map. It will be interesting to test this general rule for the mapping of other modalities in the mammalian SC using the genetic models described here.

EXPERIMENTAL PROCEDURES

Mice

CD-1, C57Bl/6, or WT littermate mice were used as controls for each experiment. Math5 mutant, β2 mutant, and Isl2-EphA3 knockin mice were generated and genotyped as previously described (Brown et al., 2000; Brown et al., 2001; Xu et al., 1999). Enucleation experiments were performed on postnatal day 6 mice anaesthetized on ice. All mouse protocols were performed in accordance with the University of California Santa Cruz and San Francisco IACUC standards.

Functional Imaging

Imaging of intrinsic optical signals was performed as described previously (Cang et al., 2008b; Kalatsky and Stryker, 2003). Briefly, adult mice were anesthetized with urethane (1.0 g/kg in 10% saline solution) supplemented with chlorprothixene (0.03 mg/kg), and a craniotomy was made in the left hemisphere. For imaging the SC, the overlying cortex was aspirated. Electrophysiological studies demonstrate that ablating or silencing visual cortex does not change receptive field properties of superficial SC neurons (Dräger and Hubel, 1976; Schiller et al., 1974). Optical images of the cortical intrinsic signal were obtained at the wavelength of 610 nm, using a Dalsa 1M30 CCD camera (Dalsa, Waterloo, Canada) controlled by custom software. A high-refresh-rate monitor (Nokia Multigraph 4453, 1024 × 768 pixels at 120 Hz) was placed 25 cm away from the animal where it subtended 70° of the contralateral visual field. Drifting thin bars (2° width and full-screen length) were displayed on the monitor. Animals were presented with horizontal or vertical bars drifting orthogonal to the axis corresponding to either the dorsal-ventral or nasal-temporal axis of the animal in order to stimulate the constant lines of elevation or azimuth, respectively.

Axon Tracing and Whole Eye Fill

Adult mice were anaesthetized by intraperitoneal injection of 100 mg/kg ketamine and 10 mg/kg xylazine. Juveniles were anaesthetized briefly on ice until tail reflex was absent. For corticocollicular projection labeling, an incision was made in the scalp to expose the skull over V1, and a hole was manually drilled in the skull using a 25-gauge needle over the desired injection site. A small amount of 1,1′-dioctadecyl-3,3,3′,3′-tetramethylindocarbocyanine (DiI) or 4-(4-(dihexadecylamino)styryl)-N-methylpyridinium iodide (DiA) (Invitrogen, Carlsbad, CA, USA) (10% in *N,N*-dimethylformamide) was injected using a handheld picospritzer (Parker Instrumentation, Cleveland) and a pulled glass

needle. For whole-eye fill, fluorescently labeled cholera toxin subunit B (CTB) (Invitrogen) was injected intraocularly. For RGC labeling, DiI was injected at focal regions intraocularly as described previously (Feldheim et al., 2000).

Fluorescent Microscopy

Two days (juveniles) or one week (adults) after injection, animals were sacrificed and intracardially perfused with ice-cold 4% paraformaldehyde in phosphate-buffered saline (PBS). Brains were dissected out, fixed overnight, and embedded in 2% agarose in PBS. Vibratome sections were cut 150 μm thick in the sagittal plane, coverslipped, and imaged using a digital camera through a 2.5X, 5X, or 10X objective on an Axioskop 2 Plus microscope (Zeiss).

Quantification and Statistics

Image quantifications were made using the ImageJ 1.38x program (NIH). For quantification of corticocollicular TZ overlap, images were thresholded by discarding pixels below the 20th percentile in intensity. Areas of retinal input and TZ were obtained from individual images, and overlapping pixels were obtained using the "AND" function. Statistical analyses were performed using the statistical software package R (R Foundation, Vienna). Statistical tests performed are indicated in the figure legends.

SUPPLEMENTAL DATA

Supplemental Data include Supplemental Experimental Procedures and four figures and can be found with this article online at http://www.cell.com/supplemental/S0092-8674(09)01049-6.

ACKNOWLEDGMENTS

This work was supported by grants from the NIH (R01-EY014689 to D.A.F., R01-EY02874 to M.P.S., R01-EY018621 to J.C., R01-NS031249 to G.L.). J.W.T. was supported by an NIH National Research Service Award Postdoctoral Fellowship (F32-EY18531). M.T.O was supported by an NIH Training Program for the Visual Sciences (T32-EY007120). We thank Bin Chen, Yi Zuo, and members of the Feldheim and Stryker labs for discussion and critical reading of the manuscript.

Received: April 10, 2009
Revised: June 23, 2009
Accepted: August 5, 2009
Published: October 1, 2009

REFERENCES

Bansal, A., Singer, J.H., Hwang, B.J., Xu, W., Beaudet, A., and Feller, M.B. (2000). Mice lacking specific nicotinic acetylcholine receptor subunits exhibit dramatically altered spontaneous activity patterns and reveal a limited role for retinal waves in forming ON and OFF circuits in the inner retina. J. Neurosci. *20*, 7672–7681.

Brown, A., Yates, P.A., Burrola, P., Ortuño, D., Vaidya, A., Jessell, T.M., Pfaff, S.L., O'Leary, D.D., and Lemke, G. (2000). Topographic mapping from the retina to the midbrain is controlled by relative but not absolute levels of EphA receptor signaling. Cell *102*, 77–88.

Brown, N.L., Patel, S., Brzezinski, J., and Glaser, T. (2001). Math5 is required for retinal ganglion cell and optic nerve formation. Development *128*, 2497–2508.

Cang, J., Kaneko, M., Yamada, J., Woods, G., Stryker, M.P., and Feldheim, D.A. (2005a). Ephrin-as guide the formation of functional maps in the visual cortex. Neuron *48*, 577–589.

Cang, J., Niell, C.M., Liu, X., Pfeiffenberger, C., Feldheim, D.A., and Stryker, M.P. (2008a). Selective Disruption of One Cartesian Axis of Cortical Maps and Receptive Fields by Deficiency in Ephrin-As and Structured Activity. Neuron *57*, 511–523.

Cang, J., Renteria, R.C., Kaneko, M., Liu, X., Copenhagen, D.R., and Stryker, M.P. (2005b). Development of precise maps in visual cortex requires patterned spontaneous activity in the retina. Neuron *48*, 797–809.

Cang, J., Wang, L., Stryker, M.P., and Feldheim, D.A. (2008b). Roles of ephrin-as and structured activity in the development of functional maps in the superior colliculus. J. Neurosci. *28*, 11015–11023.

Chandrasekaran, A.R., Plas, D.T., Gonzalez, E., and Crair, M.C. (2005). Evidence for an instructive role of retinal activity in retinotopic map refinement in the superior colliculus of the mouse. J. Neurosci. *25*, 6929–6938.

Chandrasekaran, A.R., Shah, R.D., and Crair, M.C. (2007). Developmental homeostasis of mouse retinocollicular synapses. J. Neurosci. *27*, 1746–1755.

Chiu, C., and Weliky, M. (2001). Spontaneous activity in developing ferret visual cortex in vivo. J. Neurosci. *21*, 8906–8914.

Chklovskii, D.B., and Koulakov, A. (2004). Maps in the brain: what can we learn from them? Annu. Rev. Neurosci. *27*, 369–392.

Demas, J., Sagdullaev, B.T., Green, E., Jaubert-Miazza, L., McCall, M.A., Gregg, R.G., Wong, R.O., and Guido, W. (2006). Failure to maintain eye-specific segregation in nob, a mutant with abnormally patterned retinal activity. Neuron *50*, 247–259.

Dräger, U.C., and Hubel, D.H. (1976). Topography of visual and somatosensory projections to mouse superior colliculus. J. Neurophysiol. *39*, 91–101.

Feldheim, D.A., Vanderhaeghen, P., Hansen, M.J., Frisén, J., Lu, Q., Barbacid, M., and Flanagan, J.G. (1998). Topographic guidance labels in a sensory projection to the forebrain. Neuron *21*, 1303–1313.

Feldheim, D.A., Kim, Y.I., Bergemann, A.D., Frisén, J., Barbacid, M., and Flanagan, J.G. (2000). Genetic analysis of ephrin-A2 and ephrin-A5 shows their requirement in multiple aspects of retinocollicular mapping. Neuron *25*, 563–574.

Felleman, D.J., and Van Essen, D.C. (1991). Distributed hierarchical processing in the primate cerebral cortex. Cereb. Cortex *1*, 1–47.

Feller, M.B., Wellis, D.P., Stellwagen, D., Werblin, F.S., and Shatz, C.J. (1996). Requirement for cholinergic synaptic transmission in the propagation of spontaneous retinal waves. Science *272*, 1182–1187.

Firth, S.I., Wang, C.T., and Feller, M.B. (2005). Retinal waves: mechanisms and function in visual system development. Cell Calcium *37*, 425–432.

Frisén, J., Yates, P.A., McLaughlin, T., Friedman, G.C., O'Leary, D.D., and Barbacid, M. (1998). Ephrin-A5 (AL-1/RAGS) is essential for proper retinal axon guidance and topographic mapping in the mammalian visual system. Neuron *20*, 235–243.

Gallarda, B.W., Bonanomi, D., Müller, D., Brown, A., Alaynick, W.A., Andrews, S.E., Lemke, G., Pfaff, S.L., and Marquardt, T. (2008). Segregation of axial motor and sensory pathways via heterotypic trans-axonal signaling. Science *320*, 233–236.

García del Caño, G., Gerrikagoitia, I., and Martínez-Millán, L. (2002). Plastic reaction of the rat visual corticocollicular connection after contralateral retinal deafferentiation at the neonatal or adult stage: axonal growth versus reactive synaptogenesis. J. Comp. Neurol. *446*, 166–178.

Hebb, D. (1949). The Organization of Behavior: A Neurophysiological Theory (New York: Wiley).

Hindges, R., McLaughlin, T., Genoud, N., Henkemeyer, M., and O'Leary, D.D. (2002). EphB forward signaling controls directional branch extension and arborization required for dorsal-ventral retinotopic mapping. Neuron *35*, 475–487.

Huberman, A.D., Feller, M., and Chapman, B. (2008a). Mechanisms underlying development of visual maps and receptive fields. Annu. Rev. Neurosci. *31*, 479–509.

Huberman, A.D., Manu, M., Koch, S.M., Susman, M.W., Lutz, A.B., Ullian, E.M., Baccus, S.A., and Barres, B.A. (2008b). Architecture and activity-mediated refinement of axonal projections from a mosaic of genetically identified retinal ganglion cells. Neuron *59*, 425–438.

Kalatsky, V.A., and Stryker, M.P. (2003). New paradigm for optical imaging: temporally encoded maps of intrinsic signal. Neuron *38*, 529–545.

Khachab, M.Y., and Bruce, L.L. (1999). The development of corticocollicular projections in anophthalmic mice. Brain Res. Dev. Brain Res. *114*, 179–192.

King, A.J., Hutchings, M.E., Moore, D.R., and Blakemore, C. (1988). Developmental plasticity in the visual and auditory representations in the mammalian superior colliculus. Nature *332*, 73–76.

Knudsen, E.I., and Brainard, M.S. (1991). Visual instruction of the neural map of auditory space in the developing optic tectum. Science *253*, 85–87.

Lemke, G., and Reber, M. (2005). Retinotectal mapping: new insights from molecular genetics. Annu. Rev. Cell Dev. Biol. *21*, 551–580.

Lin, B., Wang, S.W., and Masland, R.H. (2004). Retinal ganglion cell type, size, and spacing can be specified independent of homotypic dendritic contacts. Neuron *43*, 475–485.

Luo, L., and Flanagan, J. (2007). Development of continuous and discrete neural maps. Neuron *56*, 284–300.

May, P.J. (2005). The mammalian superior colliculus: laminar structure and connections. Prog. Brain Res. *151*, 321–378.

McLaughlin, T., Torborg, C.L., Feller, M.B., and O'Leary, D.D. (2003). Retinotopic map refinement requires spontaneous retinal waves during a brief critical period of development. Neuron *40*, 1147–1160.

Mesulam, M.M. (1998). From sensation to cognition. Brain *121*, 1013–1052.

Nevin, L.M., Taylor, M.R., and Baier, H. (2008). Hardwiring of fine synaptic layers in the zebrafish visual pathway. Neural Dev. *3*, 36.

Pak, W., Hindges, R., Lim, Y.S., Pfaff, S.L., and O'Leary, D.D. (2004). Magnitude of binocular vision controlled by islet-2 repression of a genetic program that specifies laterality of retinal axon pathfinding. Cell *119*, 567–578.

Pfeiffenberger, C., Yamada, J., and Feldheim, D.A. (2006). Ephrin-As and patterned retinal activity act together in the development of topographic maps in the primary visual system. J. Neurosci. *26*, 12873–12884.

Pittman, A.J., Law, M.Y., and Chien, C.B. (2008). Pathfinding in a large vertebrate axon tract: isotypic interactions guide retinotectal axons at multiple choice points. Development *135*, 2865–2871.

Rashid, T., Upton, A.L., Blentic, A., Ciossek, T., Knoll, B., Thompson, I.D., and Drescher, U. (2005). Opposing Gradients of Ephrin-As and EphA7 in the Superior Colliculus Are Essential for Topographic Mapping in the Mammalian Visual System. Neuron *47*, 57–69.

Reber, M., Burrola, P., and Lemke, G. (2004). A relative signalling model for the formation of a topographic neural map. Nature *431*, 847–853.

Sanes, J.R., and Yamagata, M. (1999). Formation of lamina-specific synaptic connections. Curr. Opin. Neurobiol. *9*, 79–87.

Schiller, P.H., Stryker, M.P., Cynader, M., and Berman, N. (1974). Response characteristics of single cells in the monkey superior colliculus following ablation or cooling of visual cortex. J. Neurophysiol. *37*, 181–194.

Singer, J.H., Mirotznik, R.R., and Feller, M.B. (2001). Potentiation of L-type calcium channels reveals nonsynaptic mechanisms that correlate spontaneous activity in the developing mammalian retina. J. Neurosci. *21*, 8514–8522.

Sperry, R.W. (1963). Chemoaffinity in the orderly growth of nerve fiber patterns and connections. Proc. Natl. Acad. Sci. USA *50*, 703–710.

Sun, C., Warland, D.K., Ballesteros, J.M., van der List, D., and Chalupa, L.M. (2008). Retinal waves in mice lacking the beta2 subunit of the nicotinic acetylcholine receptor. Proc. Natl. Acad. Sci. USA *105*, 13638–13643.

Syed, M.M., Lee, S., Zheng, J., and Zhou, Z.J. (2004). Stage-dependent dynamics and modulation of spontaneous waves in the developing rabbit retina. J. Physiol. *560*, 533–549.

Treisman, A. (1996). The binding problem. Curr. Opin. Neurobiol. *6*, 171–178.

Wolfe, J.M., and Cave, K.R. (1999). The psychophysical evidence for a binding problem in human vision. Neuron *24*, 11–17, 111–125.

Wong, R.O. (1999). Retinal waves and visual system development. Annu. Rev. Neurosci. *22*, 29–47.

Xu, W., Orr-Urtreger, A., Nigro, F., Gelber, S., Sutcliffe, C.B., Armstrong, D., Patrick, J.W., Role, L.W., Beaudet, A.L., and De Biasi, M. (1999). Multiorgan autonomic dysfunction in mice lacking the beta2 and the beta4 subunits of neuronal nicotinic acetylcholine receptors. J. Neurosci. *19*, 9298–9305.